Optics Letters

Discrete refraction and reflection in temporal lattice heterostructures

Hao Chen,[1] Chengzhi Qin,[1] Bing Wang,[1,*] and Peixiang Lu[2,3]

[1]Wuhan National Laboratory for Optoelectronics and School of Physics, Huazhong University of Science and Technology, Wuhan 430074, China
[2]Laboratory for Optical Information Technology, Wuhan Institute of Technology, Wuhan 430205, China
[3]e-mail: lupeixiang@hust.edu.cn
*Corresponding author: wangbing@hust.edu.cn

Received 3 September 2018; revised 3 December 2018; accepted 15 December 2018; posted 17 December 2018 (Doc. ID 344515); published 11 January 2019

By using a fiber loop with a phase modulator, we simulate the refraction and reflection effects of optical pulses at the heterointerface in the time domain, which is formed by abruptly varying the modulation depth or frequency. When the variation is periodically imposed on the optical pulse, the heterointerface is vertical and may lead to total internal reflection. The temporal refraction can be controlled by setting different Bloch wave vectors at incidence. As the variation occurs at a specific moment during the pulse propagation, a horizontal interface appears, and the negative refraction and pulse splitting in the time domain could be observed. We also show that the combination between the straight and tilted lattice could provide another way to control the temporal refraction. The study may find great applications in signals processing and optical communication. © 2019 Optical Society of America

https://doi.org/10.1364/OL.44.000363

Refraction and reflection are well-known phenomena that are observed when a light beam encounters an interface between two mediums with different refractive indices. As the refraction and reflection take place, the tangential momentum along the interface of the two mediums has to be conserved. Recent studies have generalized the refraction and reflection from continuous optical systems to discrete ones, including metamaterials [1,2], photonic crystals [3], and coupled waveguide arrays [4,5]. Compared to their continuous counterparts, discrete refraction and reflection manifest distinct features, such as negative refraction and refraction transparency [6,7]. The effects have provided new capabilities to control the flow of light on the subwavelength scale.

Considering the space–time duality and the analogy between spatial paraxial diffraction and temporal narrowband dispersion, the diffraction in real space can readily find counterparts in the time domain, such as time imaging and temporal Talbot effect [8]. Accordingly, the refraction and reflection have also been demonstrated in the time domain by creating an artificially temporal interface [9–11]. The refraction of the optical pulse tends to be accompanied by the wavelength conversion, which can be used to control the temporal waveform and bandwidth of optical signals. Additionally, the temporal discrete lattices have been proposed and employed to realize Bloch oscillation and discrete solitons in nonlinear optical fiber systems [12–15].

In this work, we will study the discrete refraction and reflection at a heterointerface between two distinct temporal lattices. By engineering the band structures on both sides of the interface, the refraction and reflection of the optical pulses can be artificially manipulated. The interfaces composed of temporal lattice heterostructures provide not only a flexible approach to control the propagation of the pulses by band engineering [16], but also a promising platform to demonstrate the well-known spatial behaviors of light propagation.

The proposed setup for creating the temporal lattice is shown in Fig. 1(a). The incident continuous waves convert to Gaussian pulses by using a Mach–Zehnder modulator (MZM). The temporal width of the pulses is 600 ps. A linear temporal phase variation is added upon each pulse by using the phase modulator (PM1). Then each pulse is associated with a phase factor of $\exp(ik_{T0}t)$. With the aid of the load switch, a single pulse is selected and enters the fiber loop via a 50/50 coupler. The optical delay line (ODL) is used to adjust the circulation time of the pulse in the loop. The frequency spectrum of the pulse is modulated by the phase modulator (PM2), which is driven by a radio frequency (RF) signal. The phase modulation provides a time-periodic potential [14,15,17]. The pulse also passes a dispersion-compensating fiber (DCF) with a group velocity dispersion coefficient $\beta_2 = 60 \times 10^{-27}$ s^2/m and a length $L = 1.5$ km. The effect of phase modulation and dispersion can change the temporal waveform of the pulse as the circulation times are increased. For simplicity, the dispersion of other components and higher-order dispersion are neglected. After each circulation, half of the energy of the wave packet remains in the fiber loop, and the other goes into the digital communication analyzer (DCA). The propagation loss and link power loss can be compensated by the erbium-doped fiber amplifier (EDFA) with a gain of 21 dB. The isolator is utilized to ensure unidirectional operation. The circulation times are controlled by the unload switch.

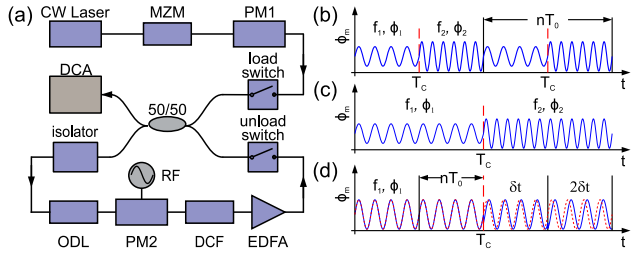

Fig. 1. (a) Schematic diagram of the fiber loop used to construct the temporal lattice. The periodic temporal potential is provided by PM2 in the fiber loop. (b) Temporal waveform of the modulation signal used to generate the vertical interface where the abrupt change occurs at $t = T_c$ in each circulation period. $\phi_{1,2}$ and $f_{1,2}$ denote the modulation depth and frequency. Each circulation time is chosen as nT_0. (c) and (d) Schematic of the modulation signal used to realize the horizontal interface. Here, $\phi_{1,2}$ and $f_{1,2}$ change only once during the whole process. The modulation signal has a time delay δt in each circulation in (d).

The evolution of the pulse can be described by the modified Schrödinger equation [18]:

$$\left\{ i\frac{\partial}{\partial z} - \frac{\beta_2}{2}\frac{\partial^2}{\partial t^2} + V_0 \cos[2\pi f(t - \alpha z)] \right\} \psi(t, z) = 0, \quad \textbf{(1)}$$

where z represents the propagation direction along the fiber loop and t is the time deviation relative to the peak of the optical pulse at $z = 0$. The slowly varying envelope approximation is satisfied since the temporal width of the pulses is as large as 600 ps. The amplitude of the temporal potential is given by $V_0 = \phi/L$, where ϕ is phase modulation depth. The modulation frequency is denoted by $f = 1/T_0$ with T_0 being the time period. α is the drift velocity of the potential along the time dimension, which indicates that the constructed temporal lattice is tilted to the t axis. The wave packet takes the form of a Bloch wave $\psi(t, z) = u(t)\exp(ik_T t)\exp(i\beta z)$, where $u(t)$ is the lattice periodic function. The propagation constant β along the z direction is the eigenvalue of Eq. (1). $k_T \in [-\pi/T_0, \pi/T_0]$ is the Bloch wave vector along the time axis. The lattice band structure is thus given by $\beta = \beta(k_T)$, which can be solved numerically with the plane wave expansion method [19].

We first consider the case of vertical interface as $\alpha = 0$. The situation can be realized as the optical length of fiber loop $L_0 = v(nT_0)$, where n is an integer, and $v = c/n_{\text{eff}}$ is the pulse propagation velocity in the fiber. The interface is constructed by employing a temporal modulation, as shown in Fig. 1(b). Within each circulation, the modulation signal experiences an abrupt change at $t = T_c$ in the modulation frequency and depth such that $f = f_1$, $\phi = \phi_1$ for $t < T_c$ and $f = f_2$, $\phi = \phi_2$ for $t > T_c$. Then, an interface vertical to the time axis can be formed, as shown in the insets of Figs. 2(a) and 2(b).

The pulse evolution in the loop is depicted in Figs. 2(a) and 2(b), which is obtained numerically by using a spit-step algorithm [14,18]. The incident pulse possesses a linear phase factor of $\exp(ik_{T0}t)$, which is imposed by PM1. As $f_1 = f_2 = 20$GHz, $\phi_1 = 0.2$, $\phi_2 = 0.3$, and $k_{T0} = 10\ \pi$GHz, the pulse experiences a deviation along the $-t$ direction at first and then splits into two pulses deviating in opposite directions in time when encountering the interface at $t = T_c$, as

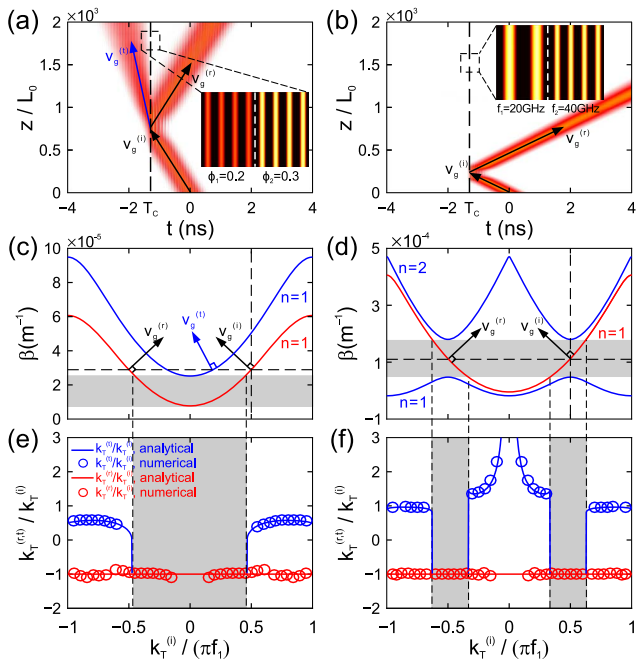

Fig. 2. (a) Evolution of the optical pulse at the vertical interface for $f_1 = f_2 = 20$ GHz, $\phi_1 = 0.2$, $\phi_2 = 0.3$, and $k_T^{(i)} = k_{T0} = 10\ \pi$GHz. (b) Evolution of the pulse at the interface for $f_1 = 20$ GHz, $f_2 = 40$ GHz, $\phi_1 = \phi_2 = 0.2$, and $k_T^{(i)} = k_{T0} = 20\ \pi$GHz. $\vec{v}_g^{(i)}$, $\vec{v}_g^{(r)}$, and $\vec{v}_g^{(t)}$ denote the group velocities of the incident, reflected, and refracted pulses in the t-z plane. Insets show the temporal lattice structures. (c) and (d) Band structures of the lattice on the right (red curve) and left (blue curve) sides of the interface, corresponding to the insets in (a) and (b). n is the band index. (e) and (f) Ratio for $k_T^{(t)}/k_T^{(i)}$ (blue curve) and $k_T^{(r)}/k_T^{(i)}$ (red curve) versus initial Bloch wave vector. The solid curves and circles represent the analytical and the numerical results. The gray regions indicate the bandgaps.

illustrated in Fig. 2(a). The process is very alike to reflection and refraction in real space. On the other hand, as $\phi_1 = \phi_2 = 0.2$, $f_1 = 20$ GHz, $f_2 = 40$ GHz, and $k_{T0} = 20\ \pi$GHz, only the reflection is observed, as shown in Fig. 2(b). The phenomena can be explained by using the band structure $\beta(k_T)$. The lattice band structures on both sides of the interface are plotted in Figs. 2(c) and 2(d). Considering the translation symmetry along the interface, the tangential wave vector along the z direction is conserved, that is,

$$\beta_I(k_T^{(i)}) = \beta_T^{(n)}(k_T^{(t)}) = \beta_I(k_T^{(r)}). \quad \textbf{(2)}$$

Here, $k_T^{(i)}$, $k_T^{(t)}$, and $k_T^{(r)}$ represent the Bloch wave vectors of the incident, refracted, and reflected pulses, respectively. β_I and β_T denote the propagation constants of the incident and transmitting lattices, and n is the band index. For the case of Fig. 2(a), the band structures of the lattices on the left and right sides of the interface are depicted by blue and red curves. The pulse is incident from the right lattice. For a definite initial Bloch wave vector $k_T^{(i)} = k_{T0} = 10\ \pi$GHz, the value β for all modes should be identical. In order to feature the deviation direction of the pulse, we introduce an effective group velocity $\vec{v}_g$, which indicates the direction of the pulse evolution in the t-z plane. By using the dispersion relation $\beta(k_T)$, it is readily to figure out

that $\arg(\vec{v}_g) = atan(-\mathrm{d}k_T/d\beta)$. Consequently, the group velocity is perpendicular to the band curves. Figure 2(c) shows the directions of $\vec{v}_g$ for the reflection and refraction, which coincides with the numerical simulations in Fig. 2(a). As the incident wave vector locates in the gray region, the bandgap of the transmitting lattice, there should not be a refracted pulse since one cannot find the same β value in the blue curve. Thus, total internal reflection (TIR) occurs, as shown in Figs. 2(b) and 2(d). The refraction can be observed either in the first band or higher bands above the gray region. The simulated $k_T^{(t)}/k_T^{(i)}$ and $k_T^{(r)}/k_T^{(i)}$ are plotted by the blue and red circles in Figs. 2(e) and 2(f), which agree with the analytical results denoted by solid lines. The shadowed region represents the situation of TIR, which refers to bandgaps in Figs. 2(c) and 2(d).

To quantitatively characterize the refraction in time, we can define the temporal relative refraction index,

$$n_r = v_{g,t}^{(t)}/v_{g,t}^{(i)}, \tag{3}$$

where $v_{g,t}^{(t)} = -d\beta_T(k_T^{(t)})/dk_T^{(t)}$ and $v_{g,t}^{(i)} = -d\beta_I(k_T^{(i)})/dk_T^{(i)}$, referring to the group velocities of the incident and refracted pulses along the time axis [16]. For the cases in Figs. 2(a) and 2(b), the relative refraction index versus the incident Bloch wave vector is shown in Figs. 3(a) and 3(b). The TIR can be realized when the initial Bloch wave vector is chosen in the gray regions, which is determined by the bandgap and the band curve of the lattice on the incident side.

Next we investigate the horizontal interface, which is realized by changing the modulation depth and frequency only once in the entire transmitting process of the optical pulse, as shown in Fig. 1(c). The parameters of the potential are changed abruptly from ϕ_1, f_1 to ϕ_2, f_2, such that an interface in the propagation direction can be formed. The interface is horizontal to the time axis, as shown in the insets of Figs. 4(a) and 4(b). In Fig. 4(a), as $\phi_1 = \phi_2 = 0.2$, $f_1 = 20$ GHz, $f_2 = 40$ GHz, and $k_{T0} = 20\ \pi$GHz, the peak of the pulse keeps constant in the lower lattice and then splits into two symmetric pulses in the upper lattice. As $f_1 = 40$ GHz, $f_2 = 20$ GHz, and $k_{T0} = 32\ \pi$GHz, the pulse experiences a deviation to the $-t$ direction in the lower lattice and then splits into three pulses with distinct amplitudes, as depicted in Fig. 4(b). It should be mentioned that the reflection of the pulse cannot be found in the horizontal case since the pulse always move forward in the z axis.

The pulse splitting can also be explained by the band structures, as shown in Figs. 4(c) and 4(d). For all the bands, the horizontal Bloch wave vector should be conserved in both lattices, namely $k_T^{(t)} = k_T^{(i)}$, which is analogous to the Floquet

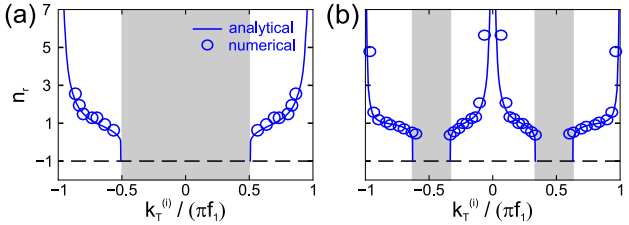

Fig. 3. (a) and (b) Relative refractive index n_r versus the incident Bloch wave vector for the situations in Figs. 2(a) and 2(b). The solid curves and circles represent the analytical and numerical results. The gray regions indicate the regimes where TIR occurs.

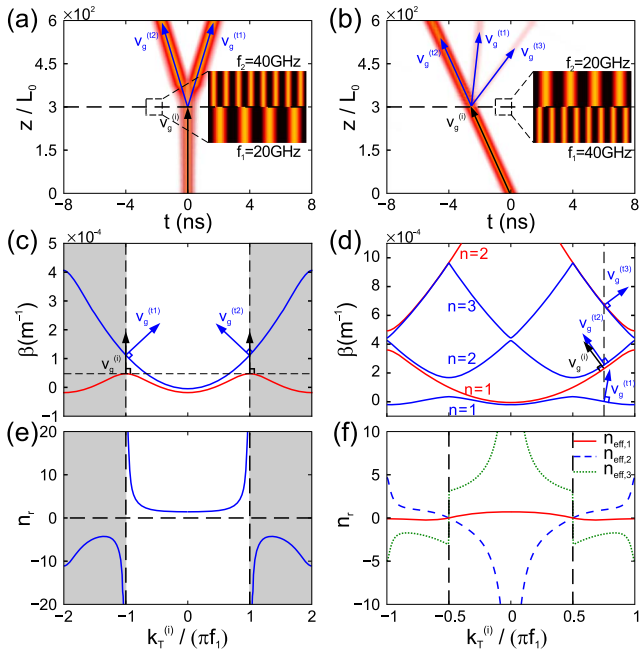

Fig. 4. Pulse splitting at the horizontal interface for (a) $\phi_1 = \phi_2 = 0.2$, $f_1 = 20$ GHz, $f_2 = 40$ GHz, $k_T^{(i)} = k_{T0} = 20\ \pi$GHz; (b) $\phi_1 = \phi_2 = 0.2$, $f_1 = 40$ GHz, $f_2 = 20$ GHz, and $k_T^{(i)} = k_{T0} = 32\ \pi$GHz. $\vec{v}_g^{(i)}$ and $\vec{v}_g^{(t)}$ refer to the group velocities of the incident and refracted pulses, denoted by the black and blue arrows. Insets represent the lattice structures. (c) and (d) Band structures of the lower (red curves) and upper (blue curves) lattices with n being the band index. (e) and (f) Relative refraction index versus initial Bloch wave vector for different bands. The gray regions indicate where the negative refraction occurs.

condition in spatial lattices. In Fig. 4(c), we consider only the bands of $n = 1$, which are isolated from higher-order bands in the two lattices. Since $f_2 = 2f_1$, the Brillouin zone of the lower lattice is repeated twice with respect to that of the upper lattice. An arbitrary Bloch wave vector from the lower lattice corresponds to two matched Bloch wave vectors in the upper one. Moreover, the time dimension group velocities for the matched wave vectors have opposite signs. Thus, the splitting occurs at the interface. As shown in Fig. 4(d), the higher-order bands of $n = 2$ and 3 of the upper lattice locate between the $n = 1$ and $n = 2$ bands of the lower lattice. An initial Bloch wave vector from the $n = 1$ band of lower lattice matches the Bloch wave vectors of $n = 1$, 2, and 3 bands in the upper lattice, giving rise to the splitting with three different refracted pulses. According to the band structures and Eq. (3), the relative refraction index versus the incident Bloch wave vector is shown in Figs. 4(e) and 4(f). The red, blue, and green lines in Fig. 4(f) correspond to $n = 1$, 2, 3 bands of the upper lattice, respectively. The predicted direction of the group velocity for each refracted pulse coincides well with the numerical simulation. It should be mentioned that the interface can also be created by abruptly changing the modulation phase. Even if the band structures are same on both sides of the interface, the reflection and refraction are observable due to the lattice defect formed by the abrupt phase change.

We turn to the situation of tilted lattice with $\alpha \neq 0$. According to Eq. (1), the tilted lattice comes from the moving

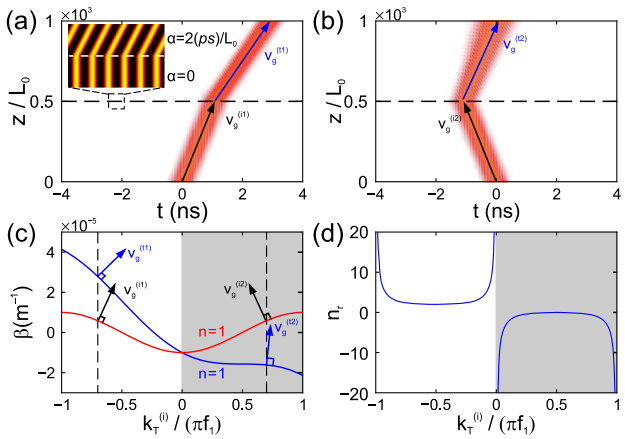

Fig. 5. (a) Positive and (b) negative refraction for the initial Bloch wave vectors $k_{T0} = -/+ 14\ \pi$GHz. $\vec{v}_g^{(i)}$ and $\vec{v}_g^{(t)}$ denote the group velocities of the incident and refracted pulses, which are denoted by the black and blue arrows. (c) Band structures of the vertical (red curve) and tilted (blue curve) lattices. (d) Relative refraction index versus the initial Bloch wave vector. The gray region indicates where the negative refraction occurs.

potential $V(t - \alpha z)$, which indicates that the center of the potential drifts along the t direction with a constant group velocity of $1/\alpha$ [6]. As illustrated in Fig. 1(d), the drift potential can be realized by tuning the optical length of the loop using the ODL, with a time delay $\delta t = \alpha L_0$ added to the RF signal in each circulation. The switching speed of the ODL should be less than the circulation time of the pulse in fiber loop, which is about 5 μs. Then, a horizontal interface can be created by cascading a perpendicular and a tilted lattice, as depicted in the inset in Fig. 5(a). The pulse is incident from the perpendicular lattice. We choose $\phi = 0.2$, $f = 20$ GHz, and $\delta t = 2$ ps. In Fig. 5(a), the optical pulse with $k_{T0} = -14\ \pi$GHz experiences a larger deviation to the t direction in the upper lattice. On the contrary, as $k_{T0} = 14\ \pi$GHz, the directions of the deviation are opposite before and after the interface, as shown in Fig. 5(b). The refraction can be explained by the band structures of the vertical and tilted lattices. According to Galilean transformation [20] and tight-binding approximation [21], in the moving reference frame of $T = t - \alpha z$ and $Z = z$, Eq. (1) reads

$$\beta_T \tilde{\psi} = -\kappa[\tilde{\psi}(T + T_0, Z) + \tilde{\psi}(T - T_0, Z)] + V(T)\tilde{\psi} - i\alpha\partial_T\tilde{\psi}, \tag{4}$$

where $\tilde{\psi} = \psi(t, z)\exp[-i(2\alpha T + \alpha^2 z)/(2\beta_2)]$. The band structure is

$$\beta_T = -2\kappa\cos(k_T T_0) + \alpha k_T, \tag{5}$$

where $\kappa = \beta_2/(2T_0^2)$ is the effective coupling coefficient. The group velocity along the time axis is thus $v_{g,t} = -d\beta_T/dk_T = -2\kappa T_0\sin(k_T T_0) - \alpha$. So, the contribution of α is an additional constant group velocity superimposed onto the original sinusoidal group velocity. The band structures of the straight and tilted temporal lattices are shown in Fig. 5(c). As $\delta t = 2$ ps, the group velocity always satisfies $v_{g,t}^{(t)} > 0$. The relative refraction index is plotted in Fig. 5(d). As the initial Bloch wave vector is chosen within the gray region such as $k_{T0} = 14\ \pi$GHz, we have $n_r < 0$, which indicates the negative refraction at the interface. On the contrary, as the initial Bloch wave vector is chosen outside the gray region, i.e., $k_{T0} = -14\ \pi$GHz, we obtain $n_r > 0$, giving rise to the positive refraction. So, we can achieve the positive and negative refractions in the same lattice heterostructure by varying the incident Bloch wave vector.

In conclusion, we have investigated the evolution of the optical pulse in an optical fiber loop with a copropagating potential. By using the abrupt change of the potential amplitude or frequency, a temporal interface appears, which is vertical or horizontal to the time axis. Additionally, the horizontal interface also can be achieved by adding a time delay to the modulation signal. By varying the incident Bloch wave vector, the TIR and negative refraction are realized at the vertical and horizontal interface, respectively. The study provides a flexible platform to manipulate the optical pulse in time by using band structures and may find great applications in signals processing and optical communication.

Funding. National Natural Science Foundation of China (NSFC) (11674117); The 973 Program (2014CB921301).

REFERENCES

1. D. R. Smith, J. B. Pendry, and M. C. Wiltshire, Science **305**, 788 (2004).
2. J. Valentine, S. Zhang, T. Zentgraf, E. Ulin-Avila, D. A. Genov, G. Bartal, and X. Zhang, Nature **455**, 376 (2008).
3. E. Cubukcu, K. Aydin, E. Ozbay, S. Foteinopoulou, and C. M. Soukoulis, Nature **423**, 604 (2003).
4. X. Fan, G. P. Wang, J. C. Lee, and C. T. Chan, Phys. Rev. Lett. **97**, 073901 (2006).
5. S. Ke, D. Zhao, Q. Liu, and W. Liu, Opt. Quantum Electron. **50**, 393 (2018).
6. S. Longhi, Opt. Lett. **42**, 5086 (2017).
7. C. Qin, F. Zhou, Y. Peng, D. Sounas, X. Zhu, B. Wang, J. Dong, X. Zhang, A. Alù, and P. Lu, Phys. Rev. Lett. **120**, 133901 (2018).
8. R. Maram, J. Van Howe, M. Li, and J. Azaña, Nat. Commun. **5**, 5163 (2014).
9. B. W. Plansinis, W. R. Donaldson, and G. P. Agrawal, Phys. Rev. Lett. **115**, 183901 (2015).
10. J. Zhou, G. Zheng, and J. Wu, Phys. Rev. A **93**, 063847 (2016).
11. B. W. Plansinis, W. R. Donaldson, and G. P. Agrawal, J. Opt. Soc. Am. B **33**, 1112 (2016).
12. A. Regensburger, C. Bersch, B. Hinrichs, G. Onishchukov, A. Schreiber, C. Silberhorn, and U. Peschel, Phys. Rev. Lett. **107**, 233902 (2011).
13. S. Wang, C. Qin, B. Wang, and P. Lu, Opt. Express **26**, 19235 (2018).
14. C. Bersch, G. Onishchukov, and U. Peschel, Phys. Rev. Lett. **109**, 282 (2012).
15. C. Bersch, G. Onishchukov, and U. Peschel, Appl. Phys. B **104**, 495 (2011).
16. C. Qin, L. Yuan, B. Wang, S. Fan, and P. Lu, Phys. Rev. A **97**, 063838 (2018).
17. Q. Liu, S. Ke, and W. Liu, Opt. Quantum Electron. **50**, 356 (2018).
18. G. P. Agrawal, *Nonlinear Fiber Optics* (Academic, 1989).
19. H. S. Sözüer, J. W. Haus, and R. Inguva, Phys. Rev. B **45**, 13962 (1992).
20. G. Rosen, Am. J. Phys. **40**, 683 (1972).
21. T. B. Boykin and G. Klimeck, Eur. J. Phys. **25**, 503 (2004).

115.156.213.246 {ts '2019-01-18 21:22:48'}